AFRL-PR-WP-TP-2007-222

COOLING PERFORMANCE OF A PARTIALLY-CONFINED FC-72 SPRAY: THE EFFECT OF VARIABLE GRAVITY (Postprint)

Travis E. Michalak, Kirk L. Yerkes, Rebekah Puterbaugh, Scott K. Thomas, and John McQuillen

JANUARY 2007

Approved for public release; distribution is unlimited.

STINFO COPY

PROPULSION DIRECTORATE
AIR FORCE RESEARCH LABORATORY
AIR FORCE MATERIEL COMMAND
WRIGHT-PATTERSON AIR FORCE BASE, OH 45433-7251

REPORT DOCUMENTATION PAGE

Form Approved
OMB No. 0704-0188

1. REPORT DATE *(DD-MM-YY)*	2. REPORT TYPE	3. DATES COVERED *(From - To)*
January 2007	Conference Paper Postprint	07/01/2004 – 12/15/2006

4. TITLE AND SUBTITLE
COOLING PERFORMANCE OF A PARTIALLY-CONFINED FC-72 SPRAY: THE EFFECT OF VARIABLE GRAVITY (Postprint)

5a. CONTRACT NUMBER
In-House

5b. GRANT NUMBER

5c. PROGRAM ELEMENT NUMBER
62203F

6. AUTHOR(S)
Travis E. Michalak, Kirk L. Yerkes, and Rebekah Puterbaugh (Power Division (AFRL/PRP))
Scott K. Thomas (Wright State University)
John McQuillen (NASA Glenn Research Center)

5d. PROJECT NUMBER
3145

5e. TASK NUMBER
20

5f. WORK UNIT NUMBER
314520C9

7. PERFORMING ORGANIZATION NAME(S) AND ADDRESS(ES)
Power Division (AFRL/PRP)
Propulsion Directorate
Air Force Research Laboratory, Air Force Materiel Command
Wright-Patterson AFB, OH 45433-7251

Wright State University
Dayton, OH 45435

NASA Glenn Research Center
Cleveland, OH 44135

8. PERFORMING ORGANIZATION REPORT NUMBER
AFRL-PR-WP-TP-2007-222

9. SPONSORING/MONITORING AGENCY NAME(S) AND ADDRESS(ES)
Propulsion Directorate
Air Force Research Laboratory
Air Force Materiel Command
Wright-Patterson AFB, OH 45433-7251

10. SPONSORING/MONITORING AGENCY ACRONYM(S)
AFRL-PR-WP

11. SPONSORING/MONITORING AGENCY REPORT NUMBER(S)
AFRL-PR-WP-TP-2007-222

12. DISTRIBUTION/AVAILABILITY STATEMENT
Approved for public release; distribution is unlimited.

13. SUPPLEMENTARY NOTES
Presented at the 45th AIAA Aerospace Sciences Meeting and Exhibit, Grand Sierra Resort Hotel, Reno, NV, 8-11 January 2007. PAO Case Number: AFRL/WS 06-2859, 14 December 2006. The U.S. Government is joint author of the work and has the right to use, modify, reproduce, release, perform, display, or disclose the work.

14. ABSTRACT
This paper discusses the effects of a variable-gravity environment on the performance of a subcooled partially-confined spray. An experiment was flown on the NASA KC-135, providing various gravity levels (- 0.16, 0.35,1.0, and 1.8 g). The experiment consists of a nozzle spraying on a Thick Film Resistor (TFR) heater which is mounted on an insulating glass pedestal. The working fluid is FC-n. Non-dimensional heat input varied over the range 35 < (1-f) GDelta < 190, with a heat flux of 20 < (l-f)q" < 70 W/cm2. The non-dimensional grouping (Frl/2Ga)l/2, a ratio of inertia and acceleration forces to viscous forces, varied over the range 35 < (Fr1/2Ga)l/2 < 70. Subcooling temperature ranged from 24° C < Tsc < 30°C. For this data, from one flight week of three flights, DeltaT = Ts-Tsat is found to decrease with decreasing values of (Fr1/2Ga)l/2. It appears that higher values for subcooling may enhance this acceleration effect. Changing the flow rate may affect how much the acceleration level affects the 2-phase heat transfer coefficient (h2-p), with the higher flow rate showing less of a change in h2-p as the acceleration level changes.

15. SUBJECT TERMS
Thermal Management, Spray Cooling, Electronics Cooling, Variable Gravity

16. SECURITY CLASSIFICATION OF:			17. LIMITATION OF ABSTRACT:	18. NUMBER OF PAGES	19a. NAME OF RESPONSIBLE PERSON (Monitor)
a. REPORT	b. ABSTRACT	c. THIS PAGE			Kirk L. Yerkes
Unclassified	Unclassified	Unclassified	SAR	20	19b. TELEPHONE NUMBER *(Include Area Code)* (937) 255-6226

Standard Form 298 (Rev. 8-98)
Prescribed by ANSI Std. Z39-18

45th AIAA Aerospace Sciences Meeting and Exhibit
8 - 11 January 2007, Reno, Nevada

AIAA 2007-198

Cooling Performance of a Partially-Confined FC-72 Spray: The Effect of Variable Gravity

Travis E. Michalak*, Kirk L. Yerkes †, Rebekah Puterbaugh‡
Air Force Research Laboratory, WPAFB OH 45433
Scott K. Thomas§
Wright State University, Dayton, OH 45435
John McQuillen¶
NASA Glenn Research Center, Cleveland, OH 44135

This paper discusses the effects of a variable-gravity environment on the performance of a subcooled partially-confined spray. An experiment, consisting of a test chamber, the associated flow loops, and instrumentation, was fabricated to be flown on the NASA Reduced-Gravity Testing Platform. This modified KC-135 aircraft was flown following a parabolic flight path to provide various gravity levels of approximately 0.16, 0.35, 1.0, and 1.8 g. The spray chamber contains two opposing nozzles spraying on Thick Film Resistor (TFR) heaters, which are mounted on insulating glass pedestals. Only the upward facing heater was used during this testing. Thermocouples under the heater in the glass pedestal and in the cooling fluid around the heater are used to determine the surface temperature and the amount of heat being carried away by the cooling fluid. The glass pedestals are surrounded by an annular sump system, which is used to collect and remove the cooling fluid from the test chamber. The fluid used for this testing is FC-72, a refrigerant that is non-toxic, non-flammable, and non-reactive. Due to its dielectric nature, FC-72 can also be sprayed directly on the electric thick film heaters. For this set of testing, the parametric ranges are as follows: The non-dimensional heat input was varied over the range $35 \le (1\text{-}f)G\Delta \le 190$, which corresponds to a heat flux to the spray of $20 \le (1\text{-}f)q'' \le 70$ W/cm^2. The non-dimensional grouping $(Fr^{1/2}Ga)^{1/2}$ was varied over the range $35 \le (Fr^{1/2}Ga)^{1/2} \le 70$, by the varying acceleration field on board the aircraft and by varying the flow rates of the cooling fluid. The working fluid is subcooled, with the subcooling temperature ranging from $24° C \le T_{sc} \le 30 °C$. The non-dimensional grouping $(Fr^{1/2}Ga)^{1/2}$ is a ratio of inertia and acceleration forces to viscous forces. For this data, which comes from one flight week consisting of three flights, the temperature difference $\Delta T = T_s\text{-}T_{sat}$ (surface temperature – saturation temperature) is generally found to decrease with decreasing values of $(Fr^{1/2}Ga)^{1/2}$ while the heat input remains constant. Similarly, from the data presented here, it appears that higher values for subcooling may enhance this acceleration effect. Also, changing the flow rate may affect how much the acceleration level affects the 2-phase heat transfer coefficient ($h_{2\text{-}\varphi}$), with the higher flow rate showing less of a change in $h_{2\text{-}\varphi}$ as the acceleration level changes.

I. Nomenclature

a	= acceleration level, g
A	= heater area, m^2
$\overline{A}, \overline{B}, \overline{C}$	= constants to be determined in surface temperature formulation
b	= radius of the glass heater post assembly, m

* Associate Mechanical Engineer, AFRL/PRPS, 1950 Fifth St. Member AIAA.
† Research Engineer, AFRL/PRP, 1950 Fifth St. Senior Member AIAA.
‡ Mechanical Engineering Co-op, AFRL/PRPS, 1950 Fifth St. Member AIAA.
§ Associate Professor, Department of Mechanical and Materials Engineering. Associate Fellow AIAA.
¶ Aerospace Engineer, Microgravity Fluid Physics Branch

D_p = droplet diameter, m
f = heater conduction loss fraction
Fr = Froude number, v^2/aD_p
g = volumetric heat generation, W/m^3, $Q/\pi b^2 H_{htr}$
G = $gb^2/((T_{sat} - T_{\infty,wall})\, k_{htr})$
$G\Delta$ = non-dimensional heat input, $q/(\pi\, b\, k_{htr}\, (T_{sat} - T_{\infty,wall}))$
Ga = Galileo number, $aD_p^3\rho^2/\mu^2$
h = convective heat transfer coefficient, W/(m^2-K)
h_{top} = convective heat transfer coefficient at surface of heater, W/(m^2-K)
$h_{1\text{-}\varphi}$ = single-phase convective heat transfer coefficient, W/(m^2-K)
$h_{2\text{-}\varphi}$ = two-phase convective heat transfer coefficient, W/(m^2-K)
H_{cov} = thickness of heater cover, m
H_{htr} = thickness of heater layer, m
H_{sub} = thickness of heater substrate, m
k = thermal conductivity, W/(m-K)
k_{cov} = thermal conductivity of heater cover, W/(m-K)
k_{fluid} = thermal conductivity of FC-72 coolant, W/(m-K)
k_{htr} = thermal conductivity of heater layer, W/(m-K)
k_{sub} = thermal conductivity of heater substrate, W/(m-K)
K = k_{fluid}/k_{htr}
Nu = Nusselt number, $h_{top}\, b/k_{fluid}$
P_{sat} = saturation pressure, N/m^2
Q = heater input power, W
Q_{cov} = power through heater cover, W
Q_{sub} = power through heater substrate, W
q'' = heater input heat flux, W/cm^2
q''_{sen} = maximum sensible heat flux, W/cm^2
$q''_{1\text{-}\varphi}$ = single-phase heat flux, W/cm^2
$q''_{2\text{-}\varphi}$ = two-phase heat flux, W/cm^2
T = temperature, °C
T_{int} = interface temperature, °C
T_b = temperature between substrate and heater, °C
T_f = free stream fluid temperature, °C
T_{noz} = nozzle inlet temperature, °C
T_s = heater surface temperature, °C
T_{sat} = saturation temperature, °C
T_{sc} = subcooling temperature, T_{sat}-T_{noz}, °C
T_{sub} = substrate temperature, °C
T_t = temperature between heater and cover, °C
$T_{\infty,top}$ = local freestream temperature of liquid flowing over heater surface, °C
$T_{\infty,wall}$ = local freestream temperature of liquid flowing along post wall, °C
v = velocity, m/s
V = volumetric flow rate, m^3/s
We = Weber Number, $\rho v^2 D_p/\sigma$
$\bar{x}$ = position variable used in surface temperature formulation

Greek symbols

ΔT = temperature difference, ($T_s - T_{sat}$), °C
θ = non-dimensional temperature, $(T - T_{\infty,wall}) / (T_{sat} - T_{\infty,wall})$
θ_{int} = $(T_{int} - T_{\infty,wall}) / (T_{sat} - T_{\infty,wall})$
θ_s = $(T_s - T_{\infty,wall}) / (T_{sat} - T_{\infty,wall})$
θ_{sat} = $(T_{sat} - T_{\infty,wall}) / (T_{sat} - T_{\infty,wall})$
$\theta_{\infty,top}$ = $(T_{\infty,top} - T_{\infty,wall}) / (T_{sat} - T_{\infty,wall})$
ρ = density, kg/m^3
σ = surface tension, kg/s^2

II. Introduction

The thermal management of high-power, high-flux devices, such as those used in power conditioning, power electronics, and directed energy applications, is becoming increasingly difficult. Even with advances in materials and efficiencies, these devices are requiring the dissipation of ever increasing amounts of thermal energy. Many of these devices also have low thermal masses and have isothermality requirements of ± 1 - 2 K. As a result, robust thermal management approaches need to be developed. Various methods have been considered, with just a few of these being two-phase flow and heat transfer[1,2] and pool boiling.[3–5] One other potential solution to the thermal management of these devices has been spray cooling.

While spray cooling is a method that has been used often in the past, there has been little research done on the effects of a variable gravity environment on the effectiveness of spray cooling. Yoshida et al.[6] and Kato et al.[7] both present some results on this topic. Some of the more recent work, however, was done by Baysinger et al.[8] These researchers presented the design and preliminary testing of a variable-gravity spray cooling experiment. The primary purpose of this study was to investigate heat transfer and fluid management issues for a continuous-flow, closed-loop spray cooling system subjected to a variable-gravity environment. Tests were conducted using ITO (Indium Tin Oxide) heaters onboard the NASA KC-135 Reduced-Gravity Research Aircraft, which provided the variable-gravity environment by following a parabolic flight trajectory. This preliminary testing provided much information on the fluid management aspects of variable gravity testing. More information on this test rig can be found in Baysinger.[9]

Building on this work by Baysinger et al.[8] was the research presented by Yerkes et al.[10] This work was again performed on the NASA KC-135 with ITO heaters, but with higher heat loads than the experiments that were presented previously. The non-dimensional heat input for these tests was varied from $(1\text{-}f)G\Delta = 30$ to 110, and the non-dimensional grouping $(Fr^{1/2}Ga)^{1/2}$ was varied from 20 to 66. During this testing, the non-dimensional temperature difference was found to decrease with decreasing $(Fr^{1/2}Ga)^{1/2}$ for a given heat load, suggesting that the Nusselt number was actually increased by decreasing $(Fr^{1/2}Ga)^{1/2}$. However, this testing was primarily in the single-phase region. It was also determined in this testing that the ITO heaters were prone to failure at the higher heat loads, due to high current densities in the thin film of resistive ITO where the heating actually takes place.

The objective of the present investigation is to continue the work presented by Baysinger et al.[8] and Yerkes et al.[10], and to investigate the effects of variable-gravity on the cooling performance of a partially-confined FC-72 spray. The experiment was again carried out using the NASA KC-135 to supply the variable gravity environment, but the ITO heaters were replaced by thick film resistor (TFR) heaters, which are capable of handling the higher heat loads. The cooling performance was tested by varying the non-dimensional heat input $35 \le (1\text{-}f)G\Delta \le 190$ for the non-dimensional grouping $35 \le (Fr^{1/2}Ga)^{1/2} \le 70$. This corresponds to a heat flux range of $20 \le (1\text{-}f)q'' \le 70$ W/cm^2. The range of subcooling for these tests was $24°C \le T_{sc} \le 30°C$.

III. Experimental Design

The experimental apparatus used in the current research is very similar to that described by Baysinger et al.[8]. This experiment consists of a test rig, which houses the fluid management and data acquisition systems, and a test chamber, which houses two opposing spray nozzles, the heater pedestal assemblies, and the fluid control / removal sump devices around the pedestals. Figure 1a) shows the entire rig, while figure 1b) shows the spray chamber. Only the upward facing heater was used during this testing.

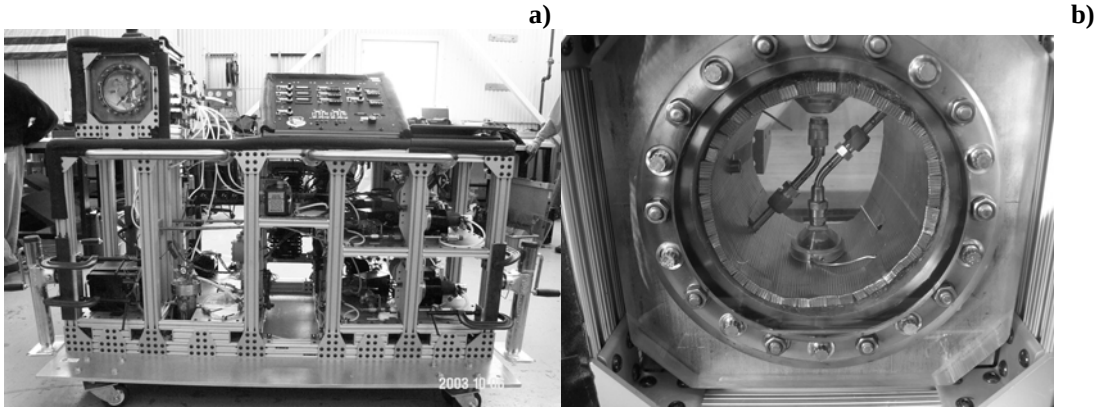

Figure 1. Experimental test rig showing the: (*a*) complete package and (*b*) test chamber.

The test rig contained three flow loops: a water loop, a spray nozzle loop, and a chamber drain loop. The water loop on this rig is used only for control of the temperature and pressure environment inside the chamber. The drain loop was used for draining the chamber, if the sumps were unable to remove sufficient fluid. The nozzle loop was used to actually deliver the working fluid, FC-72, through the spray nozzles and onto the heater surface. FC-72 was chosen as the working fluid for various reasons. It is non-toxic, non-flammable, non-corrosive, and, as a dielectric, it can be sprayed directly on the electrical component to be cooled (in this case, the TFR heater).

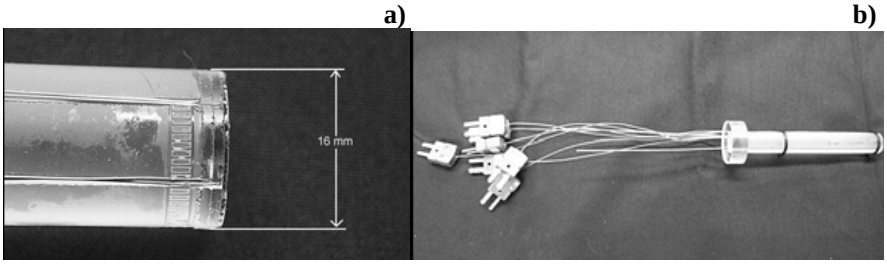

Figure 2: Pedestal photos showing: a) close-up of heater region and b) entire pedestal.

The heaters that are used in this set of testing are similar to the heater / pedestal assembly described in Yerkes et al.[10]. These cylindrical pedestals consist of several layers. The first three layers comprise the TFR heater. The layers of the TFR heater were investigated by Glaspel[11]. Table 1 summarizes the sizes and thermal conductivities of these heater layers. These heater layers sit on top of two thin wafers of glass which are each about 0.001 m thick. Finally, these glass layers sit on top of a glass pedestal, which supports and insulates the heater, in an attempt to minimize heater loss. A small (0.0254 cm diameter) Type E thermocouple is embedded between the heater substrate and the first glass layer of the pedestal. Several others of these thermocouples are embedded between the glass layers. Together, these thermocouples allow for calculations of how much heat is being lost through conduction down the glass pedestal, and what the surface temperature is at the top of the glass cover over the heater film. From the results of previous experiments, the percentage of heat being lost down the pedestal is estimated to be $f = 1.5\%$ of the total heat supplied by the heater. The pedestal was surrounded by an annular sump structure fitted with a containment cap.

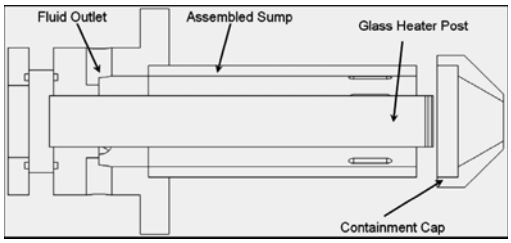

Figure 3: Pedestal in sump and cap

This sump and cap served both as fluid containment and as a means of removing the fluid from the chamber. Two thermocouples were positioned inside this sump annulus to try to monitor the temperature of the fluid that was coming off the heater. One thermocouple, the upper film temperature, was placed just off the surface of the heater, and a second, the lower film temperature, was about 1.2 cm down from the upper film temperature, near the side of the glass pedestal. These temperatures, along with the nozzle inlet temperature, allow the calculations of the average film temperature that can be used with the heater surface temperature to determine the heat transfer coefficient of the spray cooling. The nozzle inlet temperature, and therefore the subcooling of the spray, can be controlled by a preheater on the flow loop leading up to the nozzle inlet. This preheater consisted of a length of copper tubing wrapped with a heater tape, controlled by a PID temperature controller. This preheater could be used to bring the temperature of the working fluid coming out of the nozzle closer to the saturation temperature in the chamber. This saturation temperature was dictated by the pressure in the chamber, which could be controlled by the temperature of the water flowing around the chamber in the water loop.

Table 1: Heater Layer Dimensions and Conductivities

Layer	Thickness (m)	Thermal Conductivity (W / m-K)
Ceramic Substrate	$H_{sub} = 0.000634$	$k_{sub} = 27.0$
Heater	$H_{htr} = 0.000008$	$k_{htr} = 1.04$
Glass Cover	$H_{cov} = 0.000040$	$k_{cov} = 1.04$

The thermocouples in and around the pedestal in the test chamber are all referenced through a dry-well ice point to improve the stability and accuracy of the temperature readings. Additionally, the pedestal thermocouples are calibrated using an oil bath / RTD calibration setup. The acceleration of the variable gravity environment is measured by a tri-axis accelerometer mounted directly to the test chamber. All of the data that are collected from the thermocouples, the flow meters, and the pressure transducers on the flow loops

are routed through a data acquisition system to a laptop. The experiment is controlled using a control panel at the top of the test rig, next to the spray chamber.

The heater power was measured using two different voltage measurements. The first was across the heater film itself, as close to the heater as possible to minimize voltage error from the heaters leads. The second voltage measurement was across a precision resistor. This measurement allowed for the calculation of current (current = voltage / resistance). This current could then be multiplied by the voltage across the heater to give the heater power.

The data presented here was collected during one flight week on the NASA KC-135, which consisted of three flights of about forty parabolas each. Each parabola provided approximately 35 seconds of elevated gravity, followed by about 25 seconds of reduced gravity. To collect the data, the flow rate and level of subcooling were set at the beginning of the flight, and the heater power input was varied to the desired non-dimensional heat inputs. The heat level was maintained for at least one full parabola (elevated and reduced gravity), and then was adjusted to the next desired level. The set flow rate and the varying accelerations gave the varying levels for the non-dimensional grouping $(Fr^{1/2}Ga)^{1/2}$. Table 2 shows the ten various cases of flow rate, subcooling, and the non-dimensional grouping $(Fr^{1/2}Ga)^{1/2}$ for these three flights.

Table 2: Cases for the heat flux versus temperature difference plots

	Case	T_{sat} (°C)	T_{sc} (°C)	Acceleration (g)	$(Fr^{1/2}Ga)^{1/2}$	Volumetric Flow Rate $V * 10^6$ (m^3/s)	Weber Number
Flight 1	Case 1	53.7 ± 1.0	25.2 ± 1.1	0.15 ± 0.02	38.26 ± 1.26	8.70 ± 0.11	796 ± 17
	Case 2	53.7 ± 0.9	24.9 ± 1.0	1.04 ± 0.15	61.57 ± 2.53	8.63 ± 0.14	787 ± 19
	Case 3	53.5 ± 1.1	24.6 ± 1.2	1.78 ± 0.04	71.26 ± 1.00	8.73 ± 0.11	804 ± 18
Flight 2	Case 4	60.0 ± 0.3	31.3 ± 0.5	0.37 ± 0.04	47.25 ± 1.18	8.62 ± 0.09	782 ± 14
	Case 5	59.6 ± 0.4	30.5 ± 0.5	1.06 ± 0.15	61.84 ± 2.34	8.71 ± 0.05	795 ± 7
	Case 6	59.8 ± 0.5	30.8 ± 0.7	1.78 ± 0.06	70.64 ± 0.9	8.60 ± 0.07	781 ± 12
Flight 3	Case 7	59.4 ± 0.4	30.4 ± 0.7	0.16 ± 0.03	34.89 ± 1.48	6.54 ± 0.07	522 ± 7
	Case 8	59.7 ± 0.2	30.8 ± 0.4	0.36 ± 0.04	42.87 ± 1.12	6.57 ± 0.10	525 ± 7
	Case 9	58.8 ± 0.3	29.5 ± 0.5	1.06 ± 0.15	55.91 ± 2.03	6.60 ± 0.08	527 ± 8
	Case 10	59.3 ± 0.5	29.7 ± 0.5	1.76 ± 0.05	63.54 ± 0.57	6.44 ± 0.08	514 ± 7

IV. Mathematical Formulation

A. Surface temperature calculations:

The ITO (Indium Tin Oxide) heaters that were originally used on the pedestals were not capable of reaching CHF (critical heat flux) for the flow rates that were being tested. If the power was increased to try to reach CHF, the heaters failed due to the high current density in the thin film of the ITO heater. These heaters were replaced by thick film resistor (TFR) heaters. This heater consisted of a ceramic substrate, a thick film resistive element, and a glass cover plate. The thicknesses and thermal conductivities of these materials are in Table 1.

Figure 4 shows the geometry of the top of the heater pedestal (not to scale). The heat transfer through the substrate and cover are also given on this schematic, where Q is the power produced by the resistive heater and f is the fraction of heat lost down the pedestal (assumed to be 1.5%, as in previous papers). The dashed line on this plot represents the assumed temperature distribution through this TFR heater.

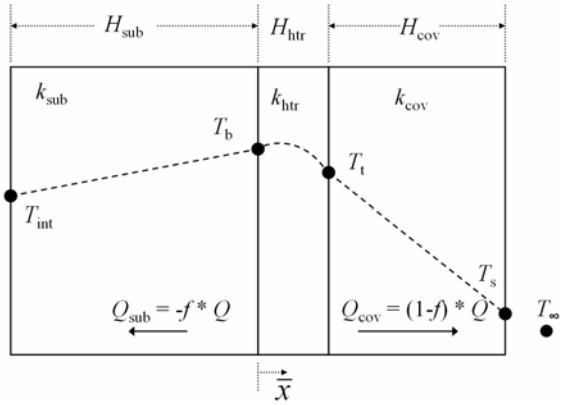

Figure 4: Heater geometry with heat flow and temperature distribution

This is based on one-dimensional heat transfer through the heater. For the purposes of reducing the data, the heater power, Q, and the temperature at the interface between the substrate and the glass pedestal, T_{int}, are known. The

temperature profiles in the substrate and cover regions are assumed to follow one-dimensional conduction, and the temperatures at the interfaces are the only relevant temperatures in this case. The following equations show the equations for these temperatures.

$$Q_{sub} = -k_{sub} A\left(\frac{T_b - T_{int}}{H_{sub}}\right) \Rightarrow \frac{dT}{dx} = \frac{T_b - T_{int}}{H_{sub}} = -\frac{Q_{sub}}{k_{sub} A}$$
$$Q_{cov} = -k_{cov} A\left(\frac{T_s - T_t}{H_{cov}}\right) \Rightarrow \frac{dT}{dx} = \frac{T_s - T_t}{H_{cov}} = -\frac{Q_{cov}}{k_{cov} A} \quad (1)$$

T_b, the temperature between the substrate and the heater, can be calculated as:

$$T_b = -\frac{Q_{sub} H_{sub}}{A k_{sub}} + T_{int} = -\frac{fQH_{sub}}{A k_{sub}} + T_{int} \quad (2)$$

The temperature distribution within the heater can be assumed to be a parabolic function in terms of the $\bar{x}$ shown on the schematic. This parabolic temperature has to match the temperatures and slopes set by the heat transfer through the substrate and cover:

$$T(\bar{x}) = \bar{A}\bar{x}^2 + \bar{B}\bar{x} + \bar{C};\ 0 \le \bar{x} \le H_{htr}$$
$$\bar{x} = 0,\ T(0) = T_b$$
$$\bar{x} = 0,\ \frac{dT}{d\bar{x}} = -\frac{Q_{sub}}{A k_{sub}} \quad (3)$$
$$\bar{x} = H_{htr},\ \frac{dT}{d\bar{x}} = -\frac{Q_{cov}}{A k_{cov}}$$
$$\bar{x} = H_{htr},\ T(H_{htr}) = T_t$$

Using the first three boundary conditions (BC) to solve for the unknown constants $\bar{A}, \bar{B}, \bar{C}$ and then substituting these back into the distribution gives:

$$T(\bar{x}) = \frac{1}{2AH_{htr}}\left(\frac{Q_{sub}}{k_{sub}} - \frac{Q_{cov}}{k_{cov}}\right)\bar{x}^2 - \frac{Q_{sub}}{A k_{sub}}\bar{x} + T_b \quad (4)$$

Now, substitute in $\bar{x} = H_{htr}$ (fourth BC) to get the value for T_t, the temperature at the interface between the heater layer and the glass cover:

$$T_t = \frac{1}{2AH_{htr}}\left(\frac{Q_{sub}}{k_{sub}} - \frac{Q_{cov}}{k_{cov}}\right)(H_{htr})^2 - \frac{Q_{sub} H_{htr}}{A k_{sub}} + T_b \quad (5)$$

The temperature at the surface of the glass cover can be given as:

$$T_s = T_t - \frac{Q_{cov} H_{cov}}{A k_{cov}} = T_t - \frac{(1-f)QH_{cov}}{A k_{cov}} \quad (6)$$

Now, substituting in the value of T_t given above and simplifying gives the surface temperature as:

$$T_s = T_b + \frac{QH_{htr}}{A}\left\{\frac{f}{k_{sub}} - \frac{1}{2}\left[\frac{f}{k_{sub}} + \frac{(1-f)}{k_{cov}}\right]\right\} - \frac{(1-f)QH_{cov}}{A k_{cov}} \quad (7)$$

This is the surface temperature that is used for the rest of the data reduction calculations.

B. Two-Phase Heat Transfer Coefficient Definition

The standard definition of a single-phase (1-φ) heat transfer coefficient $h_{1-\varphi}$ is derived from the equation for convective heat transfer, which is:

$$q''_{1-\varphi} = h_{1-\varphi}(T_s - T_f) \quad (8)$$

This leads to a heat transfer coefficient that can be defined as

$$h_{1-\varphi} = \frac{q''_{1-\varphi}}{(T_s - T_f)} \tag{9}$$

This equation is used to calculate the $h_{1\text{-}\varphi}$ for a single point of the data. Another way of looking at this is to plot q'' versus (T_s-T_f). The average heat transfer coefficient can then be viewed as being the slope of the q'' versus (T_s-T_f) curve. This is all valid for a 1- φ system. However, for this testing, and due to the subcooling, the heater surface temperature was initially below the saturation point. With increasing heat input, the surface temperature increased until it was above the saturation point. For a surface temperature above the saturation point, it was assumed that there is vapor being generated, resulting in a two-phase (2-φ) system.

The convention for a 2-φ system is to plot q'' versus (T_s-T_{sat}). For this convention, the two phase heat transfer coefficient, $h_{2\text{-}\varphi}$, can then be viewed as the slope of q'' versus ΔT. Also, this heat transfer coefficient can be determined directly using equation (12) which accounts for the sensible heating occurring at $T_s = T_{sat}$. Being able to calculate the $h_{2\text{-}\varphi}$ value directly from the data, without first plotting it and finding a curve fit and slope, can be beneficial under certain situations.

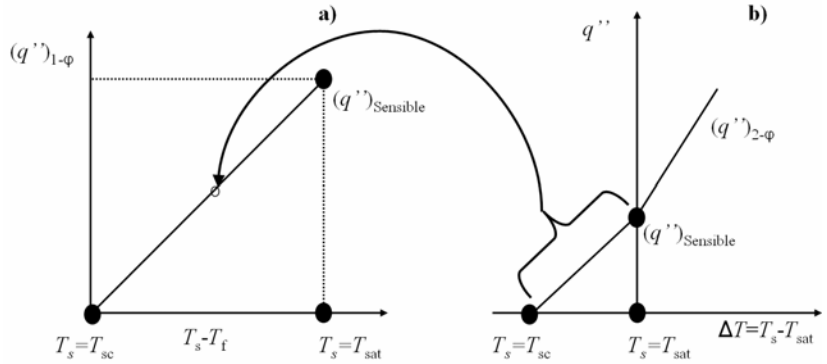

Figure 5: Heat flux versus temperature difference plots for a) single-phase and b) two-phase

Figure 5 b) shows the heat transfer curve with heat flux plotted against the temperature difference $\Delta T = (T_s\text{-}T_{sat})$. For this formulation, it was assumed that the region of $\Delta T < 0$ is single-phase, and that the region of $\Delta T > 0$ is two-phase. Thus, the 1- φ portion of this curve is basically the q'' versus (T_s-T_f) plot, figure 5 a), but transformed to a q'' versus $\Delta T = T_s - T_{sat}$ coordinate system. The heat flux at the point where the curve crosses the q'' axis ($\Delta T = 0$) is assumed to be the maximum sensible heat flux that the 1- φ fluid can achieve (here, called q''_{sen}), prior to the onset of vapor generation. The total heat flux can be calculated as:

$$q'' = h_{1-\varphi}(T_s - T_f)\Big|_{T_s=T_{sat}} + h_{2-\varphi}(T_s - T_{sat}) \Rightarrow q'' = q''_{sen} + h_{2-\varphi}(T_s - T_{sat}) \tag{10}$$

where it has been assumed that

$$h_{1-\varphi}(T_s - T_f)\Big|_{T_s=T_{sat}} = q''_{sen} \tag{11}$$

This assumption is valid if the fluid temperature and the saturation temperature remain constant. This is the case in the current research. Now, equation (10) can then be solved for $h_{2\text{-}\varphi}$ to give:

$$h_{2-\varphi} = \frac{q'' - q''_{sen}}{(T_s - T_{sat})} \tag{12}$$

This equation can then be used to calculate the two-phase heat transfer coefficient on a point by point basis, much like equation (9) calculated the single-phase heat transfer coefficient at a given point. The slope of the two-phase portion of the q'' versus ΔT curve can give the average value for the $h_{2\text{-}\varphi}$ over the entire two-phase test case.

IV. Results and Discussion

Experimental runs were conducted over the course of three flight tests as shown in Table 2. The FC-72 spray was saturated with air, approximately 30-40% by volume, based on a partial pressure calculation, to minimize maintenance of the thermal system in the event of a needed repair. However, operating the spray system with air saturated FC-72 resulted in an elevated saturation temperature that limited the maximum temperature to below onset of CHF. Table 2 describes the ten different parameter configurations that were tested during this set of three flights. For each flight, a given T_{sat}, T_{sc}, and V were set and maintained at constant levels throughout the duration of the

flight. The non-dimensional quantity $(Fr^{1/2}Ga)^{1/2}$ was varied due to the varying acceleration level on the aircraft. Figures 6-8 show the heat flux input to the spray versus the temperature difference, $\Delta T = T_s - T_{sat}$, for these ten cases. These plots are presented in both dimensional and non-dimensional form.

A. Heat Flux Versus Temperature Difference

Figure 6 a) shows the dimensional $(1-f)q''$ versus $\Delta T = T_s - T_{sat}$ plot for flight 1, while figure 6 b) gives the non-dimensional $(1-f)G\Delta$ versus $\theta_s - \theta_{sat}$ plot for this same flight. In figure 6 a), the ΔT increases with increasing heat flux, as would be expected. The left hand side of the plot (with the $(1-f)q''$ axis, $\Delta T = 0$, as the separating line) is taken to be the single-phase region, and the right hand side of the plot is taken to be two-phase. The data is plotted and linear trend lines are applied to the 1-φ and 2-φ regions separately. There is a pronounced shift in the data for the three different cases. For case 1, with the lowest value of $(Fr^{1/2}Ga)^{1/2}$, the ΔT value for any given heat flux is significantly less than the ΔT values for both case 2 and case 3 at the same heat flux. The maximum difference between the values of both V and We for these three cases is less than 3%, and the T_{sc} and T_{sat} values also change very little, on the order of 2%. The acceleration and the $(Fr^{1/2}Ga)^{1/2}$ value, on the other hand, change drastically between the three cases, and this is the only real difference between the parameters for cases 1, 2, and 3. There is some shift between cases 2 and 3, but it is not as pronounced as between cases 1 and 2. This means that between a = 0.15 g and a = 1.04 g, there is a large change, but for between a = 1.04 g and a = 1.78 g there is much less change. Another point to note is that, for this figure, there is very little difference between the slopes of the 1-φ and 2-φ regions. The data appear to be very linear throughout the entire range of ΔT. Also, the curves are relatively parallel. The curves diverge a small amount as the ΔT increases, but the slopes of the three cases are approximately the same. Many of the same trends can be seen in figure 6 b). The non-dimensional temperature difference $\theta_s - \theta_{sat}$ tends to increase as the non-dimensional heat flux $(1-f)G\Delta$ increases. There is still a difference between cases 1 and 2, showing that the lower acceleration of case 1 drops the value of $\theta_s - \theta_{sat}$ at a given $(1-f)G\Delta$ when compared to case 2. However, there is a slightly more pronounced difference between case 2 and case 3 when the non-dimensional data is observed, as compared to the dimensional data of figure 6 a). The slopes in figure 6 b) behave very similarly to those observed in 6 a), with the curves being relatively linear and parallel.

The plots for flight 2 are given in figure 7, with figure 7 a) showing the dimensional data and figure 7 b) showing the non-dimensional data. Again, the plots show both the data and linear trend lines, split up between the 1-φ and 2-φ regions. In this case, there is some difference between the slopes of the 1-φ and 2-φ regions, though it is still not a drastic change. The curves still appear to be generally linear throughout the entire range of ΔT. Also, the curves are still relatively parallel. When viewing the three different cases of figure 7, there is again a shift in the ΔT and $\theta_s - \theta_{sat}$ data. For case 4, which is at a lower acceleration (a = 0.37 g), the temperature difference is smaller at a given heat flux when compared to case 5. However, in both the dimensional and non-dimensional plots, there is more of a difference between case 5 (a = 1.06 g) and case 6 (a = 1.78 g) than between case 2 and case 3 in figure 6.

Figure 8 shows the data from flight 3. There is little difference between the two reduced-acceleration cases (case 7, at a = 0.16 g, and case 8, at a = 0.36 g). The same can be said for case 9 (a = 1.06 g) and case 10 (a = 1.76 g). There is still the familiar shift between cases 7 and 8 and cases 9 and 10. In figure 8, however, the curves do not appear to be as parallel as in figures 6 and 7. There is a good deal of divergence between cases 7 and 8 and cases 9 and 10 as ΔT increases. This suggests that there is a noticeable increase in the convective heat transfer coefficient as the acceleration level decreases.

In all of these figures, the same general trend is observed. For lower values of the non-dimensional quantity $(Fr^{1/2}Ga)^{1/2}$ (i.e., lower accelerations), the temperature difference tends to be lower for a given heat input. One initial thought was that it may have been a flow rate issue, where the flow rate was increasing at the lower acceleration levels (lower $(Fr^{1/2}Ga)^{1/2}$). However, looking at table 2, the flow rate varies by less than 3% for the different cases across each flight. For instance, the flow rates for the three different cases on flight one were all within about 0.1 m^3/s of each other. This suggests that the lowered surface temperature trend must be due to something besides a change in flow rate. The saturation temperature and the nozzle inlet temperature were both kept fairly constant over the duration of each flight (resulting in a constant level of subcooling). It is concluded that the acceleration is a major driving factor behind the change in behavior of the surface temperature (since T_{sat} remains constant).

Looking at figures 6 and 7 (flights 1 and 2) can give insight into the effect that varying the subcooling can have on the acceleration effects for this system. The volumetric flow rate for both of these flights was approximately 8 m^3/s, but the subcooling for cases 4, 5, and 6 was higher than that for 1, 2, and 3. On figure 7, the curves are spread further apart than on figure 6, as mentioned above. In other words, the reduction in the temperature difference is more pronounced in the cases with the higher subcooling. This suggests that the higher subcooling actually seems to enhance the observed acceleration effect. Also, there is more of a slope change

between the single-phase and two-phase portions of the curves in figure 7, although the curves are still relatively linear throughout the entire range of heat fluxes tested.

Comparing figures 7 and 8, the effect that varying the flow rate has on the acceleration effects can be examined. In both, there is a good deal of separation between the low-acceleration curves and the higher-acceleration curves, as would be expected with the higher subcooling. However, in figure 7, the curves are all relatively parallel, especially in the 2-phase region. There is some slope change at the ΔT=0 point, but the slopes are basically the same between the three curves. On figure 8, it appears that the lines are much less parallel, especially on the two-phase half of the curve. This means that, in flight 3, there is a higher $h_{2\text{-}\varphi}$ in the lower accelerations, since the slope of these curves is an indication of the convective heat transfer coefficient. One explanation for this is that the higher flow rate may tend to dampen out some of the effect that the acceleration has on the heat transfer coefficient in the two-phase region. In all three figures, the heat transfer coefficient (the slope) in the single-phase region is higher for the lower accelerations, which would explain why there is such a temperature difference between the lower-acceleration curves and the higher-acceleration curves. It is only in figure 8, with the lower flow rate, that this higher heat transfer coefficient carries over into the two-phase region.

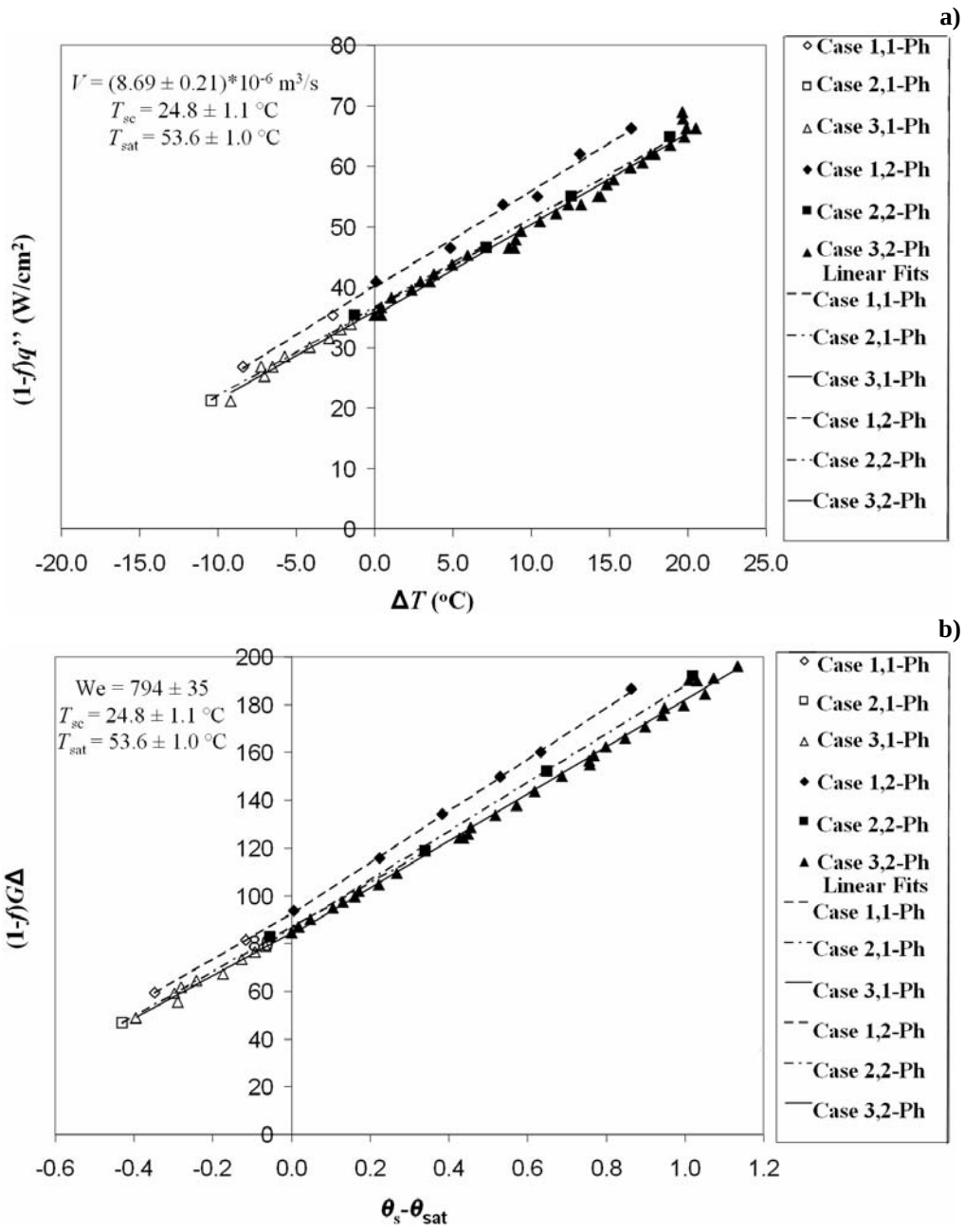

Figure 6: Heat flux to the spray versus temperature difference, T_{sc} = 24.8°C, T_{sat} = 53.6°C, V = 8.69*10^{-6} m^3/s, showing a) dimensional and b) non-dimensional formulations

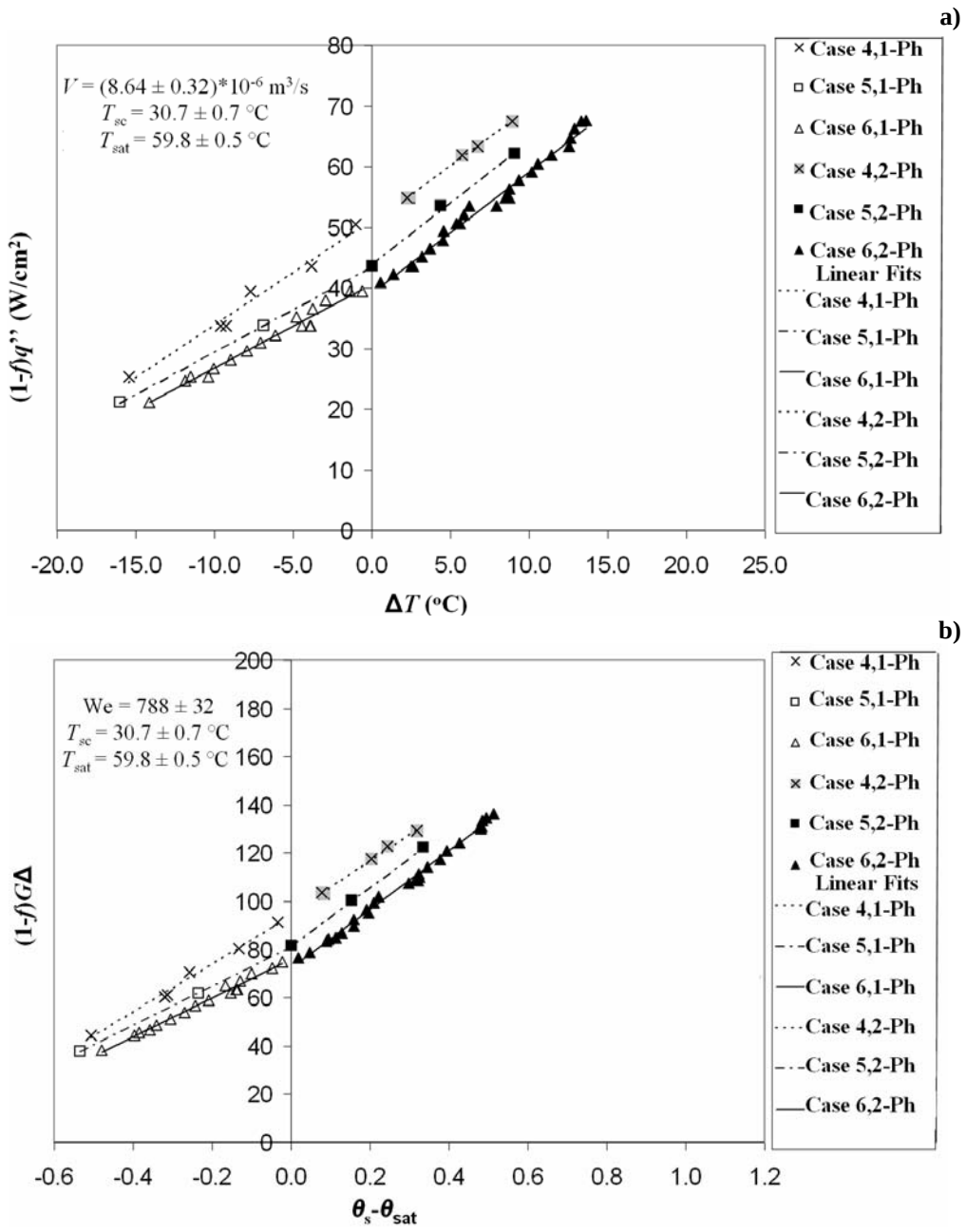

Figure 7: Heat flux to the spray versus temperature difference, T_{sc} = 30.7°C, T_{sat} = 59.8°C, V = 8.64*10^{-6} m^3/s, showing a) dimensional and b) non-dimensional formulations

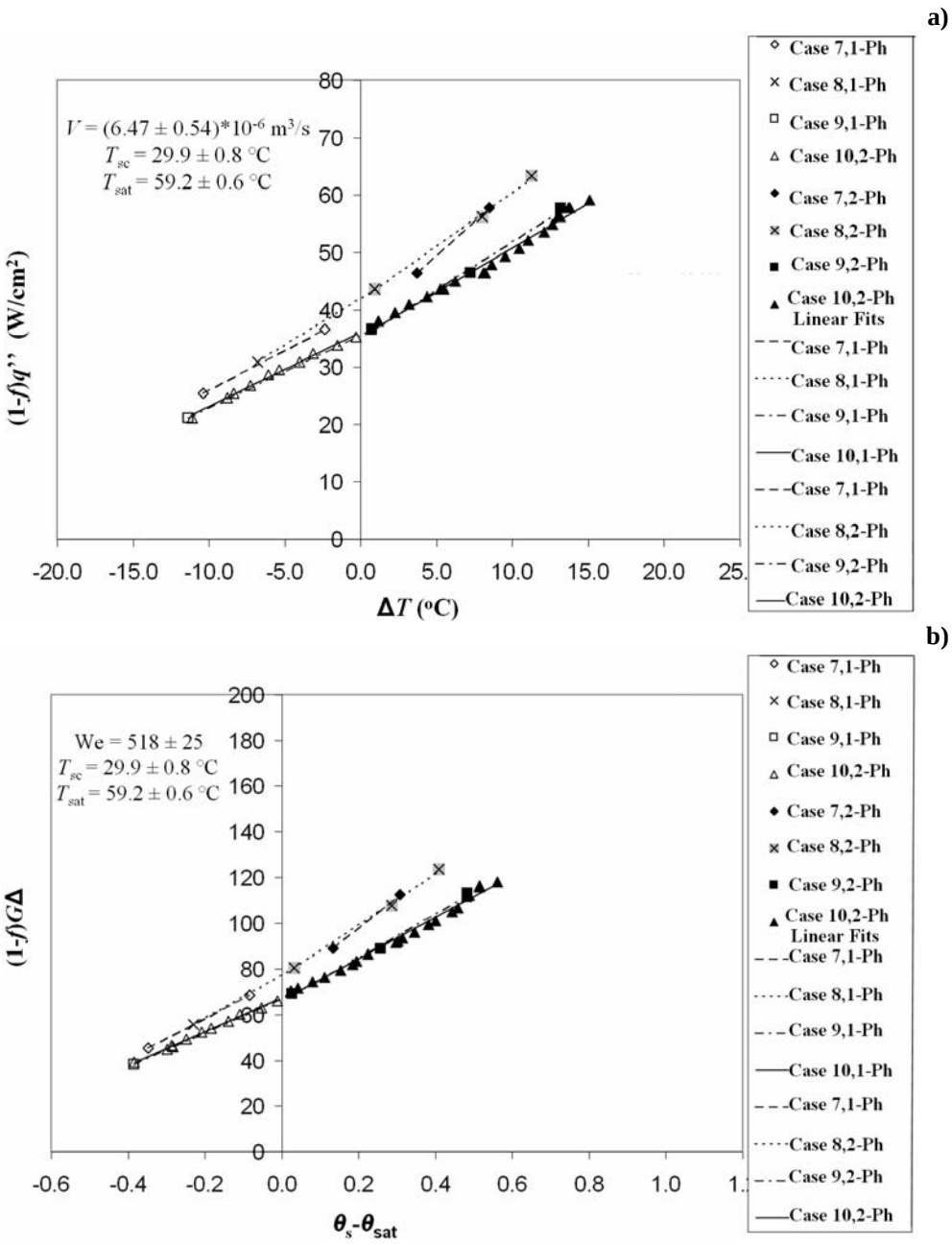

Figure 8: Heat flux to the spray versus temperature difference, T_{sc} = 29.9°C, T_{sat} = 59.2°C, $V = 6.47*10^{-6}$ m^3/s, showing a) dimensional and b) non-dimensional formulations

B. Heat Transfer Coefficient Comparison

Table 3 shows the slopes and intercepts for the various linear trend lines from figures 6 a), 7 a), and 8 a). It also shows the average and standard deviation of the calculated $h_{2\text{-}\varphi}$ value, and the percentage difference between the 2-φ slope and the average calculated $h_{2\text{-}\varphi}$ value. For each case, the calculated $h_{2\text{-}\varphi}$ value was calculated using equation (12), with the q''_{sen} value taken as the average of the 1-φ and 2-φ intercept value for that case.

Table 3: Comparison of heat transfer coefficient from calculation and slope

	Case	10000 * 1-φ Slope From q'' vs. ΔT (W/(m^2-K))	1-φ Intercept From q'' vs. ΔT (W/cm^2)	10000 * 2-φ Slope From q'' vs. ΔT (W/(m^2-K))	2-φ Intercept From q'' vs. ΔT (W/cm^2)	Average Calculated $h_{2\text{-}\varphi}$ (W/m^2-K)	Standard Deviation of Calculated $h_{2\text{-}\varphi}$	Difference: Slope and Calculated $h_{2\text{-}\varphi}$ (%)
Flight 1	Case 1	16300	40.3	16000	39.9	14800	2100	7.5
	Case 2	14500	36.5	14700	36.7	14400	1500	2.0
	Case 3	14500	35.9	15100	35.3	14900	1600	1.3
Flight 2	Case 4	17400	51.3	19100	50.6	18800	3000	1.6
	Case 5	14100	43.5	20400	43.9	23200	9300	13.7
	Case 6	13800	40.7	20100	39.1	18600	2000	7.5
Flight 3	Case 7	13900	39.9	23600	37.7	26200	11200	11.0
	Case 8	16400	42.1	18900	41.7	18600	1500	1.6
	Case 9	12800	35.6	17000	34.9	16400	1900	3.5
	Case 10	13000	36.1	15500	35.4	15000	1400	3.2

From table 3, it can be seen that the 2-phase heat transfer coefficient calculated from the slope of the q'' versus ΔT plot is very similar to the average $h_{2\text{-}\varphi}$ calculated using equation (12). The maximum percentage difference between these two values on any given case is 13.8 %. This might appear to be a fairly large difference, at first glance. However, there is a fairly large standard deviation in the calculated $h_{2\text{-}\varphi}$ values. In all ten of the cases, the slope number falls well within the range defined by the average calculated $h_{2\text{-}\varphi}$ plus or minus the standard deviation on that calculated value. The large standard deviation observed in the average calculated $h_{2\text{-}\varphi}$ is due to the general variability in the raw data. This variability in the raw data is not as evident in the slope, as it is an average value over the entire two-phase region, whereas the calculated $h_{2\text{-}\varphi}$ is an average value over just the raw points making up each individual data point. Since the slope is the heat transfer coefficient, this indicates that the method outlined above for calculating $h_{2\text{-}\varphi}$ from the data is valid.

V. Conclusions

The effects of variable gravity on the cooling performance of a partially-confined spray have been investigated. Examining the data from this flight week shows that, as the acceleration (and thus the value of $(Fr^{1/2}Ga)^{1/2}$) is decreased, there is a significant downward shift in the ΔT values, for a given $(1\text{-}f)q''$ value. This same trend is observed in the non-dimensional temperature difference and non-dimensional heat input. At this time, the physics driving the observed phenomena are not clearly understood. Similarly, from the data presented here, it appears that higher values for subcooling may enhance this acceleration effect. In addition, changing the flow rate may play a role in the extent to which the acceleration level affects the 2-phase heat transfer coefficient. The higher flow rate shows less of a change in $h_{2\text{-}\varphi}$ as the acceleration level changes. Finally, experimental data were obtained using a saturated FC-72 liquid. It is not known how dissolved air in the FC-72 affects the heat transfer with varying gravity.

In addition, the effect of variable gravity on the critical heat flux of the spray cooling was not studied in this set of tests. The interface temperature was limited by a temperature cut-off switch to try to protect the heater from over-temperature situations, and to try to keep the FC-72 from dissociating into toxic compounds. For future testing, the limit on the interface temperature can be increased, and the saturation temperature decreased by varying the chamber pressure, to allow the critical heat flux to be studied under variable-gravity conditions.

VI. Acknowledgments

This research was conducted as a collaborative effort with the NASA Glenn Research Center using the blanket interagency agreement SAA3-307 between NASA Glenn Research Center and the Air Force Research Laboratory, Order No. 12.

VII. References

[1]Mudawar, I., "Assessment of High-Heat-Flux Thermal Management Schemes," IEEE Transactions on Components and Packaging Technologies, Vol. 24, No. 2, 2001, pp. 122–141.

[2]Delil, A. A. M., "Microgravity Two-Phase Flow and Heat Transfer," Physics of Fluids in Microgravity, edited by R. Monti, Taylor and Francis, London, 2001, pp. 263–292.

[3]Kim, J., "Review of Reduced Gravity Boiling Heat Transfer: US Research," Journal of the Japan Society of Microgravity Application, Vol. 20, No. 4, 2003, pp. 264–271.

[4]Kim, J., Benton, J. F., and Wisniewski, D., "Pool Boiling Heat Transfer on Small Heaters: Effect of Gravity and Subcooling," International Journal of Heat and Mass Transfer, Vol. 45, No. 19, 2002, pp. 3919–3932.

[5]Straub, J., "Pool Boiling and Bubble Dynamics in Microgravity," Physics of Fluids in Microgravity, edited by R. Monti, Taylor and Francis, London, 2001, pp. 322–370.

[6]Yoshida, K., Abe, Y., Oka, T., Mori, Y. H., and Nagashima, A., "Spray Cooling Under Reduced Gravity Condition," Journal of Heat Transfer, Vol. 123, No. 2, 2001, pp. 309–318.

[7]Kato, M., Abe, Y., Mori, Y. H., and Nagashima, A., "Spray Cooling Characteristics Under Reduced Gravity," Journal of Thermophysics Heat Transfer, Vol. 9, No. 2, 1994, pp. 378–381.

[8]Baysinger, K. M., Yerkes, K. L., Michalak, T. E., Harris, R. J., and McQuillen, J., "Design of a Microgravity Spray Cooling Experiment," *Proc. 42nd AIAA Aerospace Sciences Conference and Exhibit*, Paper No. AIAA-2004-0966, 2004.

[9]Baysinger, K. M., "Experimental Testing and Numerical Modeling of Spray Cooling Under Terrestrial Gravity Conditions," Masters Thesis, Wright State University, Department of Mechanical and Materials Engineering, 2005.

[10]Yerkes, K.L., Michalak, T.E., Baysinger, K.M. , Puterbaugh, R.L., Thomas, S.K., and McQuillen, J., "Variable-Gravity Effects on a Single-Phase Partially-Confined Spray Cooling System," *Proc. 44th AIAA Aerospace Sciences Conference and Exhibit*, Paper No. AIAA-2006-0596, 2006.

[11]Glaspell, S.L., "Effects of the Electric Kelvin Force on Spray Cooling Performance," Masters Thesis, West Virginia University, College of Engineering and Mineral Resources, Department of Mechanical and Aerospace Engineering, 2006.